Fachtagung "Experimentelle Strömungsmechanik"
3. - 5. September 2024, Berlin

Erfassung der Reynoldsspannungen mittels Magnetresonanz-Velocimetrie – Modellannahmen im Vergleich zur LDV

Acquiring Reynolds stresses using magnetic resonance velocimetry – modeling assumptions compared to LDV

Swantje Romig[1], Kristine John[1], Martin Bruschewski[1], Sven Grundmann[1]
[1]Universität Rostock, Lehrstuhl Strömungsmechanik, Albert-Einstein-Str. 2, 18059 Rostock

Reynoldsspannungstensor, Magnet-Resonanz-Velocimetrie, Turbulenz
Reynolds stress tensor, magnetic resonance velocimetry, turbulence

Abstract

This study examines the baseline accuracy achievable in Reynolds stress tensor (RST) measurements using magnetic resonance velocimetry (MRV). Like laser Doppler velocimetry (LDV), MRV turbulence quantification relies on the assumption of an ergodic process making temporal, ensemble, and spatial averages interchangeable. Specifically, MRV assumes that the temporal variance of the velocity field can be measured as the time-averaged spatial variance within a voxel (3D pixel). This model requires that the velocity encoding process is significantly shorter than the integral time scale of the flow in these voxels. In this study, this fundamental assumption is tested in a benchmark experiment involving flow over periodic hills. The velocity autocorrelation function spectrum obtained with LDV is compared to that of the MRV velocity encoding process. Results demonstrate that when the velocity encoding process is sufficiently short, as in this experiment, MRV and LDV agree within a few percent. The residual deviation between MRV and LDV can be attributed to both techniques since LDV also applies various modeling assumptions, such as transit time weighting and optimal seeding. In conclusion, MRV provides baseline accuracy comparable to that of LDV. When laser-optical measurements are impractical, RST measurements with MRV are a reliable gold standard.

1. Introduction

Measuring the Reynolds stress tensor (RST) is desirable to quantify turbulent flows. It is also known as the temporal covariance matrix of the velocity vector with six independent components. There are several experimental methods to acquire turbulence parameters. The current gold standards are hot-wire anemometry and laser Doppler velocimetry (LDV). But they also have some drawbacks. They need physical or optical access to the flow field, are 1D measurement methods, and their data rates are low in coincidence mode (Tropea et al., 2007). Particle image velocimetry and particle tracking velocimetry achieve high data rates for 3D turbulence data but are prone to high random errors (Wilson & Smith, 2013). Optical measurement methods additionally require seeding. Magnetic Resonance Velocimetry (MRV) does not need optical access, 3D measurements are possible in a comparably short time and no seeding is needed (Elkins & Alley, 2007). In MRV all components of the RST can be encoded separately, hence no coincidence filtering is necessary (Zwaart & Pipe, 2013). Of course, MRV turbulence quantification is also based on some assumptions.
In this study, LDV and MRV measurements were performed on the same experimental setup: a periodic hill channel. First, the assumptions for MRV and LDV turbulence quantification are

GALA e.V., Karlsruhe, Germany, ISBN 978-3-9816764-4-0

explained. Then, the experimental setup is described. The validity of some MRV assumptions is checked in the Results section, where MRV and LDV results are also compared.

2. Turbulence quantification using MRV and LDV

Both measurement methods used to quantify the RST in this study rely on several assumptions presented in this section.

2.1 MRV

The signal acquired by an MRI scanner is a complex signal consisting of magnitude and phase in each voxel (3D pixel) of the whole measurement volume. It arises from the excited quantum spins of hydrogen nuclei in the examined fluid. Using a bipolar magnetic field encoding gradient, the signal's phase can be sensitized to the fluid's velocity. In the case of an intravoxel velocity distribution with finite width, as in turbulent flows, after applying the encoding gradients, the nuclear spins exhibit different phases that add up incoherently, leading to signal attenuation. This effect relates the spatial variance of the velocity within one voxel to the first moment of the magnetic field encoding gradients M_1(Gao & Gore, 1991).
MRI turbulence quantification relies on the assumption of a stationary flow. As stationary flows can always be considered ergodic (Tropea et al., 2007), the velocity's spatial variance inside a voxel is equivalent to its temporal variance.
It is also assumed that the magnetic field gradients encode the complete spectrum of the respective flow. This is achieved with very short encoding times of the MRI scanner compared to the Lagrangian integral time scale of the flow (Dyverfeldt et al., 2009). Dillinger et al. (2022) looked at the spectrum of the flow encoding gradient and the spectrum of the flow derived from the autocorrelation function in theory and showed that only if the cut-off frequency of the flow encoding gradient spectrum is high enough, it encodes the whole spectrum with all flow scales present.
Due to the spatial resolution of magnetic resonance imaging, where one voxel reflects the average of all spins inside the voxel, homogeneity of the flow inside the voxel is assumed or an average inside the voxel is acquired. Additionally, a measured 2D plane in MRV always has a finite thickness. The homogeneity assumption includes that no mean velocity gradient is present inside a voxel (Dyverfeldt et al., 2009).
Current methods for RST measurement using MRV also assume a Gaussian velocity distribution inside a voxel (Dyverfeldt et al., 2009). This leads to the following expression for the signal magnitude inside a voxel (Schmidt et al., 2021):

$$|S(\boldsymbol{k_u})| = |S(0)|\exp\left(-\frac{1}{2}\boldsymbol{k_u^T}\boldsymbol{\Sigma^{-1}}\boldsymbol{k_u}\right)$$

where $\boldsymbol{k_u} = \gamma\left[M_{1,x}, M_{1,y}, M_{1,z}\right]^T$ is the encoding vector and $M_{1,i}$ are the gradient moments in the ith direction, sensitizing the MR signal to the flow velocity. γ is the gyromagnetic ratio, $|S(\boldsymbol{k_u})|$ and $|S(0)|$ are the signal's magnitude for an encoded and a reference measurement, $\boldsymbol{\Sigma}$ is the variance of the 3D Gaussian and $\boldsymbol{\Sigma^{-1}}$ yields the RST.

2.2 LDV

Some comparable assumptions are made in LDV. While a signal is received from a particle it is assumed to have a constant velocity (Buchhave et al., 1979). When calculating the variance over a certain period stationary flow is implicitly assumed during this period. Also, the ensemble average is interpreted as a temporal average implying ergodicity. Like in MRV, a mean velocity gradient inside the measurement volume leads to an apparent turbulence intensity, and for inhomogeneous velocity distributions, an average over the measurement volume is acquired

GALA e.V., Karlsruhe, Germany, ISBN 978-3-9816764-4-0

(Buchhave et al., 1979). Note, that the measurement volume in LDV is usually smaller than a voxel in MRV.
A major topic in LDV is the velocity bias. More particles with higher velocities will cross the measurement volume in a given time than particles with lower velocities. This leads to a bias in the mean velocity and the estimated variance. Many methods have been developed to overcome this issue, where transit time weighting is the standard now as it works reliably under all flow conditions (Damaschke et al., 2018), (Edwards, 1987). Nevertheless, some assumptions are made during the derivation of transit time weighting. Statistically uniform seeding with particle rates much higher than the inverse turbulent time scale is crucial and a constant velocity inside the measurement volume is assumed or an average velocity is measured (Buchhave et al., 1979). Damaschke et al. (2018) also mentioned that the particle's path through the measurement volume influences its transit time for a nonuniform measurement volume.

3. Experimental setup and methods

The experimental setup is similar to the Ercoftac case 81 "Flow over periodic hills" (Temmerman & Leschziner, 2001), (Jang et al., 2002), and was modified to fit into the MRI scanner. It consists of 15 consecutive hills. The field of view (FOV) is between the 12th and the 13th hill. Fig. 1 depicts the measurement setup. Two 5.5 kW pumps circulate purified water from a 1000 L tank with a flow rate of 255 L/min at 22°C. The resulting Reynolds number of 29,500 is based on the hill height and the axial bulk flow velocity at the hill crest. 1 g/L copper sulfate was added for the MRV experiments and Vestosint with 5µm particle size for the LDV experiments. The flow rate, pressure, and temperature were monitored using respective sensors. For a more detailed description of the setup refer to Schmidt et al. (2021).

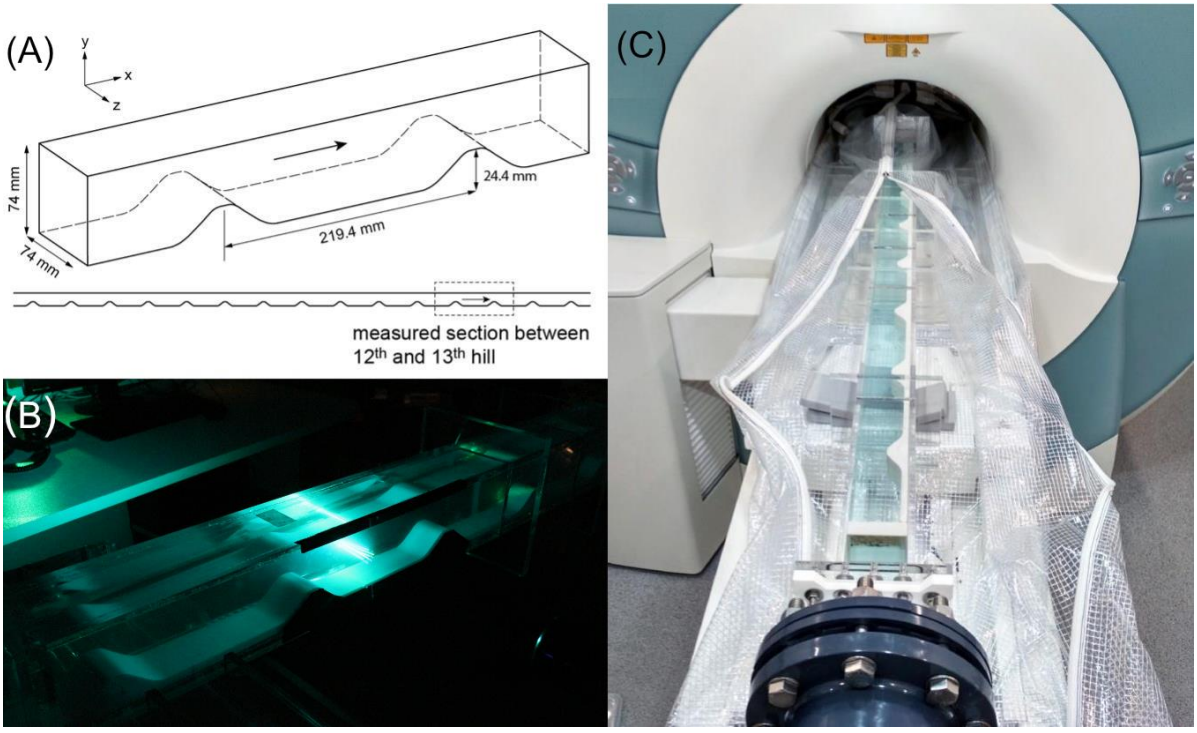

Fig. 1: Experimental setup: (A) schematic of the periodic hills, (B) LDV measurement, (C) MRV measurement.

GALA e.V., Karlsruhe, Germany, ISBN 978-3-9816764-4-0

3.1 MRV measurements

A 3T MRI system (Magnetom Tim Trio, Siemens, Germany) with 40 mT/m maximum gradient amplitude and 200 T/m/s maximum slew rate was used for the MRV measurements. A phase-contrast Gradient recalled Echo sequence with gradient design according to Bernstein et al. (1992) was used. A high receiver bandwidth of 920Hz/pix and an asymmetric readout gradient with an echo asymmetry of 0.1 was employed to minimize the sequence timing. The data was combined with the data acquired using a second asymmetric inverted readout gradient to yield complete information about the flow field. The data was averaged 128 times for low uncertainty and 10 M_1 values were used to cover the whole dynamic range of the flow. The ICOSA6 scheme (Haraldsson, et al., 2018) was employed to encode six independent directions necessary to acquire all six components of the RST. For further details of the sequence, refer to Schmidt et al. (2020) and Schmidt et al. (2021). The investigated 2D FOV was 496 mm by 120 mm with a resolution of 1 mm with a slice thickness of 6 mm. The measurements were done in 4 h11 min. The reconstruction was done using Matlab 2022b (The Mathworks, Natick, USA). First, the data from the four receiver coils was combined using sensitivity maps calculated via the ESPIRiT approach (Uecker, et al., 2014). The RST was found using a weighted least squares fit of a 3D Gaussian to the data. The reconstruction is further described by Schmidt et al. (2021), the weights were obtained according to Dyverfeldt et al. (2009).

3.2 LDV measurements

The LDV data was acquired in the same FOV as the MRV data using a FiberFlow system (Dantec dynamics, Skovlunde, Denmark) with a 2-velocity component setup in coincidence mode and 250 mm optics. The measurement volume was a rotational ellipsoid with a diameter of 0.2 mm and a length of about 3 mm. Six lines along the channel height with 0.5 mm step size were measured. 15,000 to 85,000 valid coincidence samples within 100 s dwell time were collected. Additionally, a 2D slice with a resolution of 2 mm was measured (see Fig. 4). From the velocity components u and v, the RST components $\overline{u_x{'}u_x{'}}$, $\overline{u_y{'}u_y{'}}$ and $\overline{u_x{'}u_y{'}}$ were calculated employing transit time weighting to remove the velocity bias. The data was processed using the BSA Flow Software (Dantec dynamics, Skovlunde, Denmark) and Matlab 2022b (The Mathworks, Natick, USA).
The arrival time quantization (Nobach, 2022) was used to obtain the velocity autocorrelation function (ACF) spectrum and validate the assumption that the MRV gradients encode the full spectrum of the flow. The parameters were 0.01 s temporal resolution of the ACF and 50 samples for each side of the spectrum.

4. Results

4.1 MRV assumptions

First, the flow encoding gradient spectrum and the velocity ACF spectrum derived from the LDV data according to Nobach (2022) are illustrated in Fig. 2. Note, that MRV data is acquired in the spatial frequency domain, called k-space, and that the gradients vary over k-space. The spectrum of the velocity encoding gradient is here calculated in the center of k-space for the maximum M_1 = 50 mT/m ms^2 in the y-direction because the gradient in the x-direction varies during acquisition. The gradients also vary for the encoding directions of the ICOSA6 scheme, here the encoding direction with the maximal gradient in the y-direction is chosen. The velocity ACF from LDV data is thus also calculated for the velocity component in the y-direction u_y. The position was chosen in the highly turbulent region at x = 60 mm and y = 23.5 mm. The obtained velocity ACF spectrum is noisy. For a higher resolution, more data samples would be needed. Still, the typical inertial range of a turbulent flow with a slope of -5/3 can be seen in the detailed view on the right side of Fig. 2. The flow encoding gradient spectrum covers the

GALA e.V., Karlsruhe, Germany, ISBN 978-3-9816764-4-0

full velocity spectrum of the flow as its cut-off frequency is well above the ACF spectrum cut-off frequency.

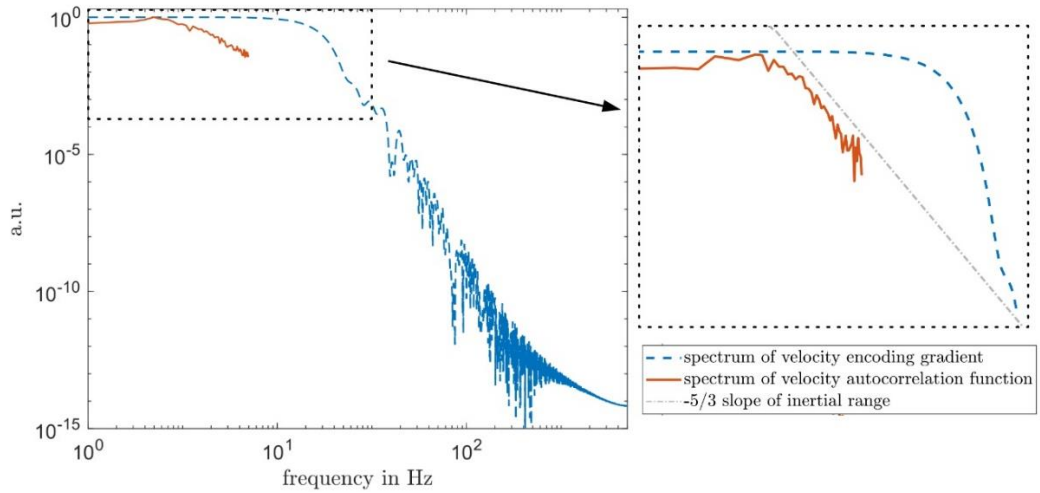

Fig. 2: Normalized spectra of the velocity encoding gradient (blue, dashed), the velocity ACF for u_y at x = 60 mm, y = 23.5 mm (red, solid), and the -5/3 slope of the inertial range (grey, dash-dotted), detailed view on the right.

Fig. 3 illustrates the reconstruction of the MRV data for two exemplary voxels in a highly turbulent region and a less turbulent region of the flow. Their positions are marked in part (A). A projection of the 3D Gaussian fit to the data is depicted in part (D). The error bars denote the standard deviation of all 128 averages. The fit is overall good, while some outliers occur for the blue voxel in the highly turbulent region at $\Delta M_1 > 30\ \mathrm{mT/m \cdot ms^2}$. They are close to the noise floor and weighted very low in the fit. Parts (B) and (C) show the effect of the intravoxel mean velocity gradient. In (B) no mean velocity gradient was assumed, in (C) a linear intravoxel mean velocity gradient was assumed and corrected for as proposed by Dyverfeldt et al. (2009) using mean velocity data also acquired via MRV. The arrow at the hill crest indicates the area that was mainly influenced by this correction. Instead of a very high turbulence level as in part (C) a very low turbulence level is indicated in part (D). In other areas of the flow, the intravoxel mean velocity gradient does not significantly influence the measured turbulence statistics.

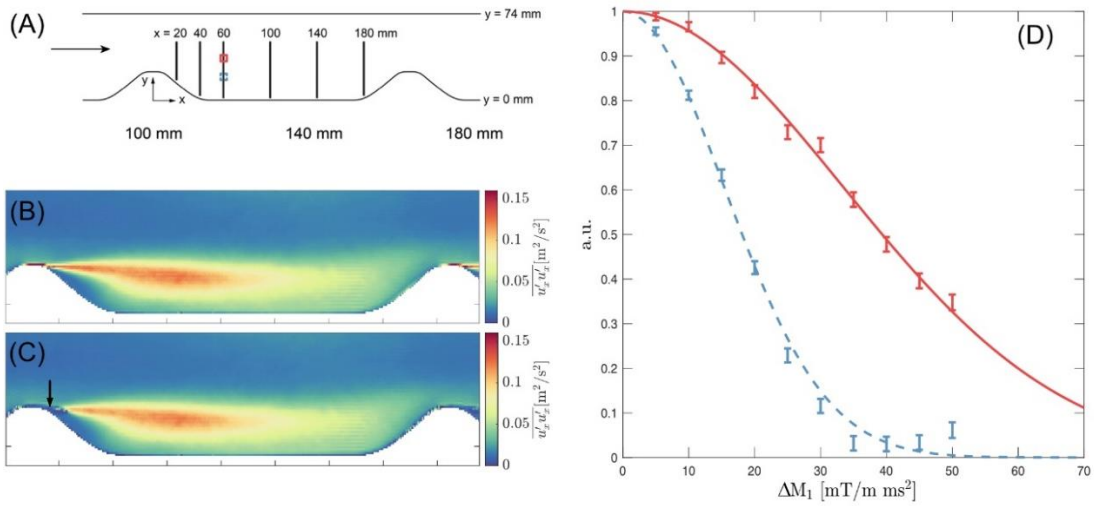

Fig. 3: 3D Gaussian fit to measured relative magnitudes (D), positions of voxels marked in (A). (B): $\overline{u_x{'}u_x{'}}$ assuming no intravoxel mean velocity gradient, (C): $\overline{u_x{'}u_x{'}}$ corrected for intravoxel mean velocity gradients according to (Dyverfeldt, Gårdhagen, Sigfridsson, Karlsson, & Ebbers, 2009).

GALA e.V., Karlsruhe, Germany, ISBN 978-3-9816764-4-0

4.2 Comparison of MRV and LDV data

In Fig. 4 the MRV and the LDV data are compared qualitatively in the 2D field. LDV and MRV data agree very well. The uncertainty for the MRV data was calculated using the dual acquisition approach described by Bruschewski et al. (2016). Therefore, the RST is reconstructed from two data sets each consisting of half of the averages acquired. The uncertainty is found as the standard deviation between both calculated RST as 0.0013 m²/s² for $\overline{u_x{'}u_x{'}}$, 0.0012 m²/s² for $\overline{u_y{'}u_y{'}}$ and 0.001 m²/s² for $\overline{u_x{'}u_y{'}}$ which is considered low as the maximum stresses are about 0.15 m²/s². At the hill crest $\overline{u_x{'}u_x{'}}$ is very high in the MRV data which can be attributed to an intravoxel mean velocity gradient. LDV does not provide data in this region directly at the wall.

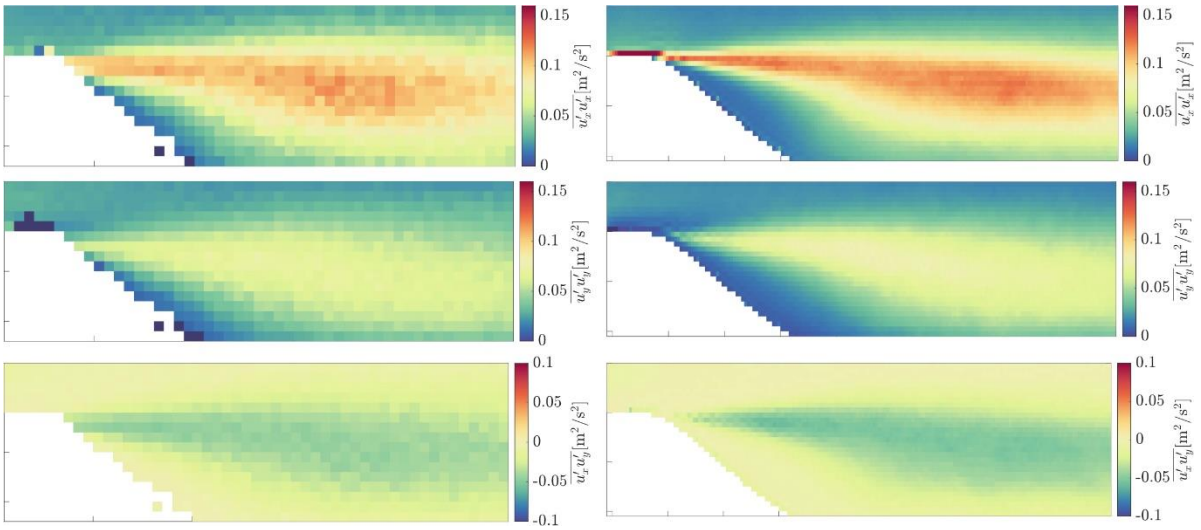

Fig. 4: RST components acquired using LDV (left) and MRV (right).

Finally, Fig. 5 allows a more quantitative comparison of the RST components acquired at selected positions downstream of the hill using MRV and LDV. The impression from Fig. 4 is confirmed. Only minor deviations of maximal 0.01 m²/s² between RST components from the MRV and the LDV data can be seen.

5. Discussion and Conclusion

Some assumptions in MRV turbulence quantification are examined for a dataset obtained for a flow over periodic hills. One of the central assumptions in MRV turbulence quantification is that the flow encoding time is short enough for the velocity field not to change during encoding time. This can be checked by looking at the spectra of the velocity encoding gradients and the velocity ACF in Fig. 2. Note, that only one position in the flow field was examined, which was chosen where the highest integral time scales can be expected. The MRV velocity encoding gradient spectrum was also investigated for one specific position in k-space. A calculation for the whole k-space would be very cumbersome and out of the scope of this study. Still, for the examined flow, the calculated gradient spectrum covers the full velocity ACF spectrum confirming the assumption and making this MRV technique feasible to measure the turbulence statistics of this flow.

The validity of the Gaussian assumption made for MRV can be checked qualitatively for two representative voxels in Fig. 3. The fitted Gaussian curves match the measured data well apart from the points close to the noise floor whose influence during the fit is restricted using the weights. Thus, the Gaussian model seems to represent this flow accurately. The very high normal stresses measured at the hill crest are located inside the shear layer, where intravoxel

GALA e.V., Karlsruhe, Germany, ISBN 978-3-9816764-4-0

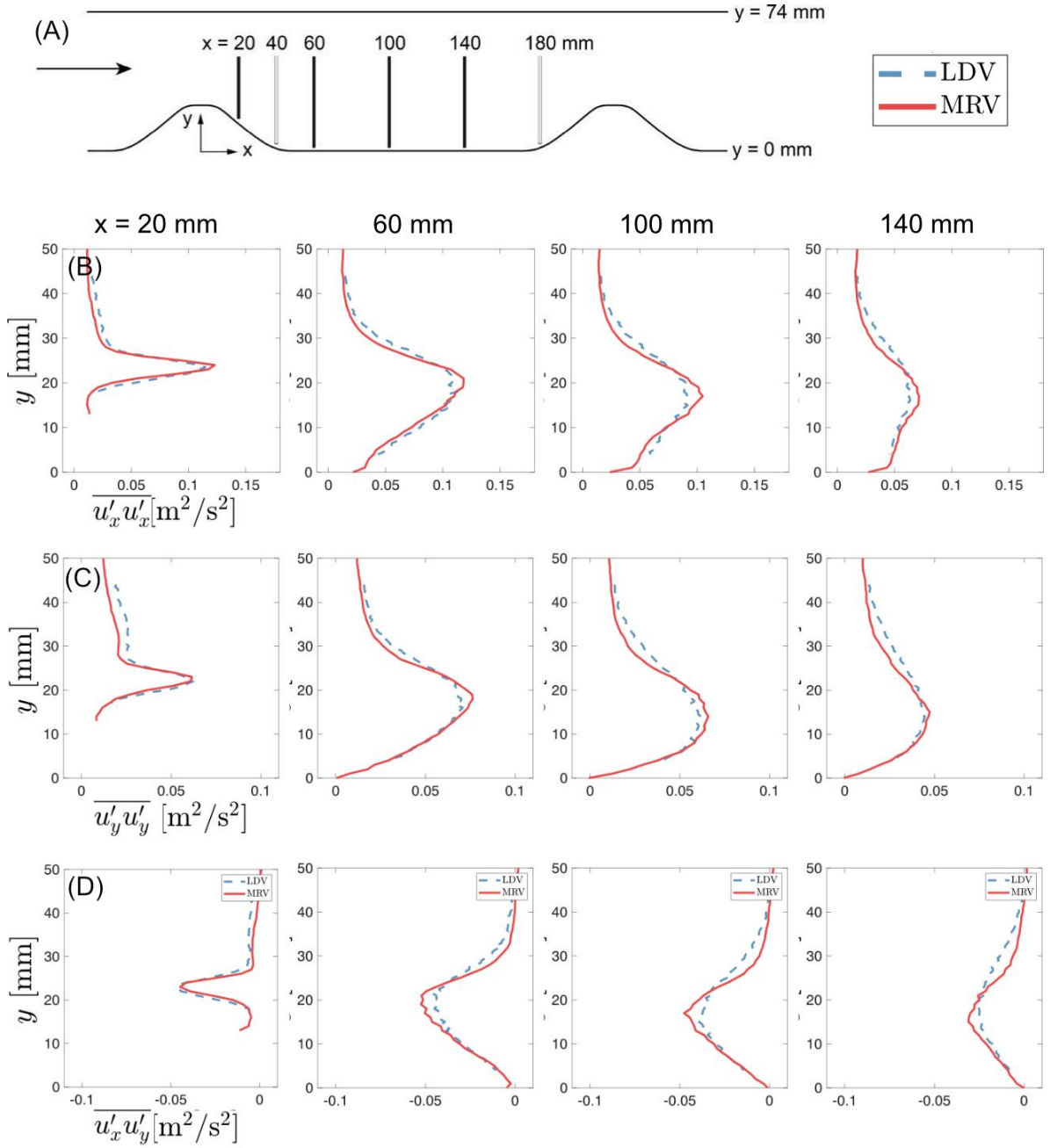

Fig. 5: Comparison of MRV and LDV RST data at selected lines, (A) positions of the selected lines, data at grey lines is not shown.

mean velocity gradients are likely present. The normal stress is estimated to be very low with the correction based on a linear mean velocity gradient, see Fig. 3 (D). Especially when compared to the LDV data in Fig. 4 the correction seems to lead to an underestimation of the RST component. In this case, the model of a linear mean velocity gradient inside the voxel might not be accurate.

Data obtained using MRV and LDV on the same flow setup is compared. As Fig. 5 shows the data agrees very well. It can be concluded, that both measurement techniques are equally capable of capturing the turbulence statistics for the examined flow and that the modeling degree and accuracy of MRV with the Gaussian velocity distribution assumption and LDV with transit time weighting for assumed statistically uniform particle concentration are comparable for this experiment. In conclusion, MRV can serve as a gold standard to validate CFD or experimental data where laser-optical measurements are impractical.

GALA e.V., Karlsruhe, Germany, ISBN 978-3-9816764-4-0

References

Bernstein, M. A., Shimakawa, A., & Pelc, N. J. (1992). Minimizing TE in moment-nulled or flow-encoded two-and three-dimensional gradient-echo imaging. *Journal of Magnetic Resonance Imaging*(5), pp. 583-588. doi:10.1002/jmri.1880020517

Bruschewski, M., Freudenhammer, D., Buchenberg, W. B., Schiffer, H. P., & Grundmann, S. (2016). Estimation of measurement uncertainty in magnetic resonance velocimetry based on statistical models. *Experiments in Fluids, 57*. doi:10.1007/s00348-016-2163-3

Buchhave, P., George, W. K., & Lumley, J. L. (1979). The measurement of turbulence with the Laser-Doppler Anemometer. *Annual Reviews Fluid Mechanics, 11*, pp. 443-503.

Damaschke, N., Kühn, V., & Nobach, H. (2018). A fair review of non-parametric bias-free autocorrelation and spectral methods for randomly sampled data in laser Doppler velocimetry. *Digital Signal Processing, 76*, pp. 22-33.

Dillinger, H., McGrath, C., Guenthner, C., & Kozerke, S. (2022). Fundamentals of turbulent flow spectrum imaging. *Magnetic Resonance in Medicine, 87*(3), pp. 1231-1249. doi:10.1002/mrm.29001

Dyverfeldt, P., Gårdhagen, R., Sigfridsson, A., Karlsson, M., & Ebbers, T. (2009). On MRI turbulence quantification. *Magnetic resonance imaging, 27*(7), pp. 913-922. doi:10.1016/j.mri.2009.05.004

Edwards, R. V. (1987). Report of the Special Panel on statistical particla bias problems in laser anemometry. pp. 89-93.

Elkins, C. J., & Alley, M. T. (2007). Magnetic resonance velocimetry: applications of magnetic resonance imaging in the measurement of fluid motion. *Expermients in Fluids, 43*, pp. 823-858.

Gao, J.-H., & Gore, J. C. (1991). Turbulent flow effects on NMR imaging: Measurement of turbulent intensity. *Medical Physics, 18*(5), pp. 1045-1051. doi:10.1118/1.596645

Haraldsson, H., Kefayati, S., Ahn, S., Dyverfeldt, P., Lantz, J., Karlsson, M., . . . Saloner, D. (2018). Assessment of Reynolds stress components and turbulent pressure loss using 4D flow MRI with extended motion encoding. *Magnetic resonance in medicine, 79*(4), pp. 1962-1971. doi:10.1002/mrm.26853

Jang, Y. J., Leschziner, M. A., Abe, K., & Temmerman, L. (2002). Investigation of anisotropy-resolving turbulence models by reference to highly-resolved LES data for separated flow. *Flow, Turbulence and Combustion, 69*, pp. 161-203. doi:10.1023/A:1024764307706

Nobach, H. (2022). Laser Doppler Data Processing. Accessed 7 June 2024, http://ldvproc.nambis.de/programs/mLDV.html.

Schmidt, S., Flassbeck, S., Bachert, P., Ladd, M. E., & Schmitter, S. (2020). Velocity encoding and velocity compensation for multi-spoke RF excitation. *Magnetic Resonance Imaging, 66*, pp. 69-85. doi:10.1016/j.mri.2019.11.007

Schmidt, S., John, K., Kim, S. J., Flassbeck, S., Schmitter, S., & Bruschewski, M. (2021). Reynolds stress tensor measurements using magnetic resonance velocimetry: expansion of the dynamic measurement range and analysis of systematic measurement errors. *Experiments in Fluids, 62*(6), p. 121. doi:10.1007/s00348-021-03218-3

Temmerman, L., & Leschziner, M. A. (2001). Large eddy simulation of separated flow in a streamwise periodic channel constriction. (pp. 399-404). New York: Begel House Inc. doi:10.1615/TSFP2.2300

Tropea, C., Yarin, A. L., & Foss, J. F. (2007). *Handbook of Experimental Fluid Mechanics.* Berlin: Springer.

Uecker, M., Lai, P., Murphy, M. J., Virtue, P., Elad, M., Pauly, J. M., . . . Lustig, M. (2014). ESPIRiT—an eigenvalue approach to autocalibrating parallel MRI: where SENSE meets GRAPPA. *Magnetic resonance in medicine, 71*(3), pp. 990-1001. doi:10.1002/mrm.24751

Wilson, B. M., & Smith, B. L. (2013). Uncertainty on PIV mean and fluctuating velocity due to bias and random errors. *Measurement Science and Technology, 24*(3), p. 035302.

Zwaart, N. R., & Pipe, J. G. (2013). Multidirectional high-moment encoding in phase contrast MRI. *Magnetic Resonance in Medicine, 69*(6), pp. 1553-1563.

GALA e.V., Karlsruhe, Germany, ISBN 978-3-9816764-4-0